Abnormal State Detection of OLTC Based on Improved Fuzzy C-means Clustering

Hongwei Li[1], *Lilong Dou*[1], *Shuaibing Li*[2*], *Yongqiang Kang*[2], *Xingzu Yang*[2] *and Haiying Dong*[2]

(1. School of Automation and Electrical Engineering, Lanzhou Jiaotong University, Lanzhou 730070, China;
2. School of New Energy and Power Engineering, Lanzhou Jiaotong University, Lanzhou 730070, China)

Abstract: An accurate extraction of vibration signal characteristics of an on-load tap changer (OLTC) during contact switching can effectively help detect its abnormal state. Therefore, an improved fuzzy C-means clustering method for abnormal state detection of the OLTC contact is proposed. First, the wavelet packet and singular spectrum analysis are used to denoise the vibration signal generated by the moving and static contacts of the OLTC. Then, the Hilbert-Huang transform that is optimized by the ensemble empirical mode decomposition (EEMD) is used to decompose the vibration signal and extract the boundary spectrum features. Finally, the gray wolf algorithm-based fuzzy C-means clustering is used to denoise the signal and determine the abnormal states of the OLTC contact. An analysis of the experimental data shows that the proposed secondary denoising method has a better denoising effect compared to the single denoising method. The EEMD can improve the modal aliasing effect, and the improved fuzzy C-means clustering can effectively identify the abnormal state of the OLTC contacts. The analysis results of field measured data further verify the effectiveness of the proposed method and provide a reference for the abnormal state detection of the OLTC.

Keywords: On-load tap changer, singular spectrum analysis, Hilbert-Huang transform, gray wolf optimization algorithm, fuzzy C-means clustering

1 Introduction

As an indispensable part of the power system, the power transformer with an OLTC is particularly important for the regulation of the system voltage. Therefore, condition monitoring of the OLTC plays a vital role in the operation and maintenance of the power transformer. In the past five years, frequent OLTC failures reported by the China Southern Power Grid Corporation and the State Grid Corporation of China have gained the attention of both industry and academia. According to the statistics, the faults induced by the OLTC account for 20% of all types of the on-load tapping transformer faults in China and 41% in European countries [1-2]. Among all the factors that result in OLTC failures or faults, the mechanical failures induced by the drive springs and other components account for more than 95% [3-4]. Therefore, to ensure a safe operation of the on-load tapping transformer, an analysis of the mechanical characteristics of the OLTC can be helpful for an abnormal state signal extraction and fault diagnosis.

Because vibration signals contain a large amount of information for characterizing the mechanical state of the power equipment, collecting vibration signals from the OLTC and other power equipment to monitor and diagnose the operation condition state has gained significant attention in this field. In Ref. [5], an acoustic vibration analysis method for the OLTC mechanical state feature extraction was proposed. Fault diagnosis of the OLTC can be achieved using the extracted features from the signal collected while the transformer is energized. In Ref. [6], Seo et al. indicated that certain power companies in Australia, Canada, and European countries have adopted vibration measurement methods to perform online condition monitoring of the OLTC of power transformers. The change in the OLTC state can be

Manuscript received April 8, 2021; revised May 17, 2021; accepted June 15, 2021. Date of publication March 31, 2023; date of current version July 20, 2021.
* Corresponding Author, E-mail: lishuaibing1105@163.com
Digital Object Identifier: 10.23919/CJEE.2023.000002

evaluated by comparing the vibration signals collected under different working states. In Ref. [7], a wavelet transform-based method was proposed for the OLTC vibration signal feature extraction, while Ref. [8] proposed using the wavelet entropy and the empirical mode decomposition (EMD) entropy to compare and analyze OLTC vibration signals. Other methods such as K-means clustering and the Hilbert transform were also proposed to analyze and classify the mechanical signals of the OLTC [9-10]. The EMD algorithm, which has been applied for signal analysis for a long time [11-13], was also introduced to detect the mechanical state of the OLTC [14-15].

In addition to the aforementioned methods or algorithms, including the wavelet transform analysis, EMD, Hilbert transform, and K-means clustering, other methods such as the Fourier transform [16], deep belief network (DBN) [17-18], wavelet and modal analysis [19], and expert system [20] were proposed for analyzing the vibration signals of the OLTC. Considering that the OLTC vibration signal originating from contact switching is a nonlinear non-stationary signal, conventional methods can analyze and process this type of signal to a certain extent; however, limitations remain in the algorithms. For example, the short-time Fourier transform and wavelet transform are capable of analyzing the non-stationary signal [12]; however, they cannot escape the limitation of the fundamental wavelet. Generally, the EMD is applied to analyze and process nonlinear and non-stationary signals, which is an effective tool for adaptive signal processing in both the time and frequency domains [13]. For the contact switching vibration signal of the OLTC, the EMD can overcome the limitation of time-based wavelet analysis if the processed signal is close to pure white noise. Evidently, the analyzed signal is not pure white noise, which makes the analysis results prone to modal aliasing. Therefore, further analysis and improvement are needed. For the K-means clustering algorithm, it is necessary to manually predetermine the K value [14], which increases the complexity and uncertainty of the algorithm. Similarly, the uncertainty of the fuzzy C-means (FCM) clustering algorithm is that the initial clustering centers are randomly generated [15]; therefore, it is easy to fall into the local optimum in the clustering process, resulting in the decline of the clustering accuracy.

To further improve the diagnosis accuracy of OLTC mechanical faults, this thesis proposes the use of wavelet packets (WP) to denoise the collected vibration signals as the first step, and the singular spectrum analysis (SSA) is applied for secondary denoising. Considering that the EMD is prone to modal aliasing when decomposing non-pure white noise, the ensemble EMD (EEMD) is adopted to decompose the denoising signal. Thereafter, the improved Hilbert-Huang transform (IHHT) is used to extract the characteristics of the OLTC vibration signal, and finally, the optimized FCM clustering algorithm is used to classify the abnormal state of the OLTC contact. Based on this, an OLTC contact failure experimental platform is designed and built to verify the effectiveness of the proposed method. Field measurements of OLTC signals are collected and analyzed for further validation. The remainder of this thesis is organized as follows. Section 2 introduces the experimental platform for simulating the OLTC contact switching. The proposed method and its implementation are detailed in Section 3, while the verification with onsite measured signals is described in Section 4. The conclusions are finally presented in Section 5.

2 Laboratory experimental platform of OLTC contact switching

For a transformer with an OLTC, the contact condition of the OLTC plays a vital role in its normal operation; the monitoring and assessment of its operating status is necessary and urgent for power companies. Generally, the fault signals of the OLTC include mechanical vibration signals and electrical signals. In contrast, the mechanical vibration signal can be used to characterize the typical failures or abnormal states of the OLTC, including contact wear, contact loosening, spindle deformation, and drive spring failures. Among these, the most common failures are contact wear and contact loosening. Therefore, a laboratory test system for simulating an actual OLTC operation is built, as shown in Fig. 1. The system includes the following two parts, which are described in detail in the subsequent sections: ① Contact switching

device; ② Data acquisition system.

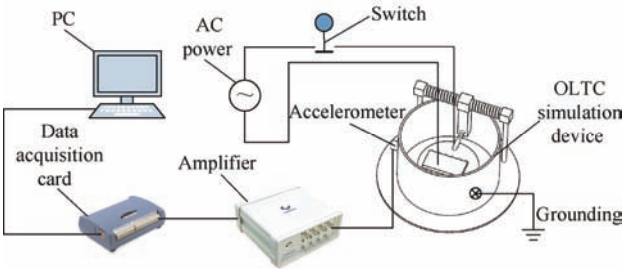

Fig. 1 Schematic of OLTC switching signal acquisition system

2.1 Contact switching device

The contact switching device consists of ① a pair of contacts, one of which is a moving contact and the other is fixed, ② a sliding lead screw mechanism driven by a motor, ③ a transformer oil-filled iron bucket to simulate the tank shell of the transformer, ④ an insulation support base made of epoxy resin board, and ⑤ a controller. The moving contact is installed in a moving slider controlled by a DC motor (12 V, 5 W) and integrated with the sliding lead screw, while the static contact is fixed on the insulating board at the bottom of the iron bucket. Both the moving and static contacts are immersed in the transformer oil. By controlling the movement of the slider and adjusting the distance between the moving and static contacts using the controller, the actual operating scene of the OLTC contacts can be simulated. Details regarding the subparts of the contact switching device are provided in Tabs. 1-3.

Tab. 1 Parameters of the moving and the static contact

Type	Material	Length/mm	Diameter/mm
Moving	Silver-copper alloy	30	20
Fixed	Silver-copper alloy	20	20

Tab. 2 Parameters of the iron bucket

Diameter/mm	Height/mm	Oil level/mm	Thickness/mm
500	300	200	3

Tab. 3 Parameters of the sliding lead screw

Length/mm	Maximum speed/(m/s)	Minimum speed/(m/s)	Vibration frequency/Hz
50	150	10	452

2.2 Data acquisition system

In the OLTC contact switching signal acquisition system, the subsystem for data acquisition consists of the following four parts: ① acceleration sensor, ② high-speed data acquisition card, ③ amplifier, and ④ host computer with data acquisition and analysis software. Detailed parameters of the acceleration sensor, high-speed data acquisition card, and the amplifier are provided in Tabs. 4-6.

Tab. 4 Parameters of the acceleration sensor

Type	Manufacture	Bandwidth/Hz	Excitation current/mA
CT1005LC	CHENGTEC	0.5-8 000	2-10

Tab. 5 Parameters of the high-speed data acquisition card

Type	Manufacture	Maximum sampling rate/(kS/s)	Number of sampling channels
MCC1608G	CHENGTEC	250	4

Tab. 6 Parameters of the amplifier

Type	Manufacture	Bandwidth/kHz	Number of sampling channels
CT5204	CHENGTEC	1-100	4

During contact switching, the vibration signals generated by the contacts can be collected by the acceleration sensor and delivered to the high-speed data acquisition card through the amplifier. Following hardware filtering and simple preprocessing by the high-speed data acquisition card, the vibration signals are finally sent to the host computer for display and analysis.

The OLTC contact wear is simulated by artificially rubbing the contact surface with sandpaper prior to conducting the moving test using the contact switching device, whereas the OLTC contact loosening is mainly simulated by the artificial loosening of the moving contact of the device. To better collect the vibration signal during contact switching, three acceleration sensors are uniformly installed around the outer wall of the iron bucket in sequence (120° apart in the horizontal plane). To simulate the operation of OLTC contacts to be similar to reality, the dynamic and static contacts in the contact switching device are made of silver copper alloy containing 2% silver, which is the material of OLTC contacts used in actual transformers. Similarly, the Karamay #25 mineral oil is selected as the insulating medium for immersing the static contact.

3 Experimental test result analysis

To ensure the stability of the output voltage, the transformer OLTC needs to be adjusted for voltage regulation with load variation. During the current-carrying and voltage-regulating operation, the dynamic and fixed contacts of the diverter switch will collide, wear, and ablate. The friction and collision of the moving and fixed contacts are the main sources of vibration signals; however, the vibration of the transformer core and winding also produces vibration signals, which makes the measured vibration signal more complex and ultimately reduces the accuracy of the abnormal state detection and fault diagnosis results. Therefore, it is critical to analyze the propagation process of the vibration signal and denoise the final collected vibration signal.

The vibration signal generated by the friction and collision of dynamic and static contacts first spreads over a certain distance in the insulating oil in the iron bucket, and then reaches and passes through the inner and outer wall of the iron bucket. Because the inner wall of the iron bucket is relatively smooth, the vibration signal will be refracted and reflected, which makes the vibration signal collected by the acceleration sensor more complicated. However, the damping of mineral oil can reduce the complexity of the vibration signal to a certain extent. The vibration of the iron core and winding also produces vibration signals in the transformer tank when the transformer is running; thus, the vibration signals measured by the external speed sensor installed on the outer wall of the iron bucket are more complex. In addition, when the dynamic and fixed contacts of the OLTC switch are switched, arc power generation will occur. The arc decomposes the mineral oil to produce C_2H_2, H_2, C_2H_4, and other fault gases [17], which metamorphose the mineral oil, reduce the insulation strength of the mineral oil, affect the arc extinguishing ability and the transmission of the vibration signal, and thus increase the complexity and difficulty of the mechanical vibration signal acquisition. Therefore, the vibration signal collected by the acceleration sensor requires signal denoising to obtain a vibration that can more accurately reflect the operating state of the OLTC. The flow of the vibration signal collection, processing, and analysis is shown in Fig. 2.

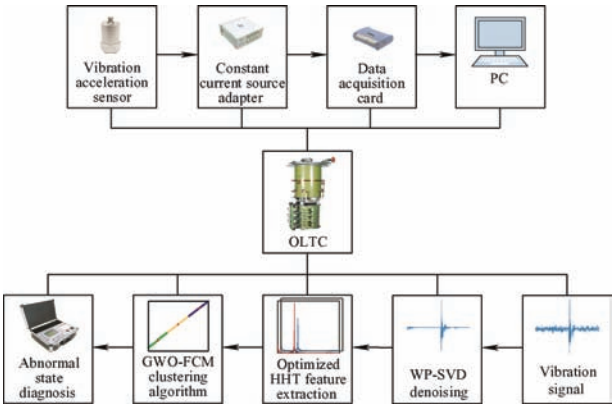

Fig. 2 Flow chart of vibration signal collection and analysis

As shown in Fig. 2, once the vibration signal is received by the host computer, the following three additional steps will be implemented for further analysis of the abnormal state detection: signal denoising using WP transform and SAA (WP-SSA), feature extraction using IHHT, and gray wolf optimizer (GWO)-based FCM clustering (GWO-FCM) for the abnormal state classification. Details regarding the four steps are provided in the following sections.

3.1 WP-SSA based signal denoising

In this thesis, the WP-SSA [18-19] is proposed to denoise the vibration signal, where the WP transform is used for the first denoising while the SSA is used for secondary denoising. The WP overcomes the shortcoming of the wavelet transform, which cannot decompose high-frequency signals. When WP is used to decompose the signal, it decomposes the signal layer-by-layer according to the decomposition scale from low to high, and all sub-band signals in each layer are decomposed into low-frequency and high-frequency components. This decomposition process is called the WP tree [19]. After the n-layer decomposition, a pure low-frequency component and 2^n high-frequency components are finally obtained. In this study, the db3 wavelet basis is used as the WP basis function and the Shannon wavelet is selected, while the number of layers for the vibration signal decomposition is determined to be five through a trial-and-error process. In addition, the window length for SSA is selected as 63. Thereafter, the signal denoised by WP is subjected to the secondary denoising using SSA. Generally, the SSA is used to remove small noise disturbances in the signal [20-21]. While maintaining the signal characteristics as far as possible, it improves the denoising accuracy and meets the

requirements of secondary denoising. Its denoising principle is as follows.

First, the one-dimensional data of the signal are constructed into a two-dimensional Hankel matrix. Let the signal to be processed be $X=[x(1), x(2),\cdots,x(N)]$, which can be formed into an $m\times n$ dimensional Hankel matrix [17] as follows

$$\boldsymbol{A}=\begin{bmatrix} x(1) & x(2) & \cdots & x(n) \\ x(2) & x(3) & \cdots & x(n+1) \\ \vdots & \vdots & & \vdots \\ x(m) & x(m+1) & \cdots & x(N) \end{bmatrix} \tag{1}$$

where, m and n should satisfy the condition of $n\geqslant m\geqslant 2$, and $m+n-1=N$.

Once SSA is performed on the Hankel matrix $\boldsymbol{A}$, its decomposition form can be written as follows [19]

$$\boldsymbol{A}=\boldsymbol{U}\boldsymbol{\Sigma}\boldsymbol{V}^{\mathrm{T}} \tag{2}$$

where $\boldsymbol{A}$ is an $m\times n$ matrix, $\boldsymbol{U}$ is an $m\times m$ orthogonal matrix, and $\boldsymbol{V}^{\mathrm{T}}$ is an $n\times n$ unitary matrix. $\boldsymbol{\Sigma}$ is a diagonal matrix of singular values of the order $m\times n$.

Singular values are usually used to express the information contained in the matrix, and the amount of information contained is positively correlated with the magnitude of the singular values. The singular values in $\boldsymbol{\Sigma}$ are arranged in descending order, and their values decay rapidly [22]. Therefore, by choosing an appropriate threshold value and preserving the first few singular values with large values, the singular diagonal matrix can be reconstructed to achieve the purpose of noise reduction. When using the SSA for secondary denoising, the vibration signal is first formed into a singular value matrix (with singular values in the diagonal). Because the singular values are usually used for describing the information contained in the matrix that represents a positive correlation, the diagonal matrix of the singular values can be reconstructed by choosing an appropriate threshold and retaining the singular values of the previous several large values.

To verify the effectiveness of the method proposed in this study, the sine and cosine functions are used to construct the original analog signal, which is followed by adding Gaussian white noise to form an analog noisy signal, and then using WP and SSA for secondary noise reduction. The noise reduction results are shown in Fig. 3.

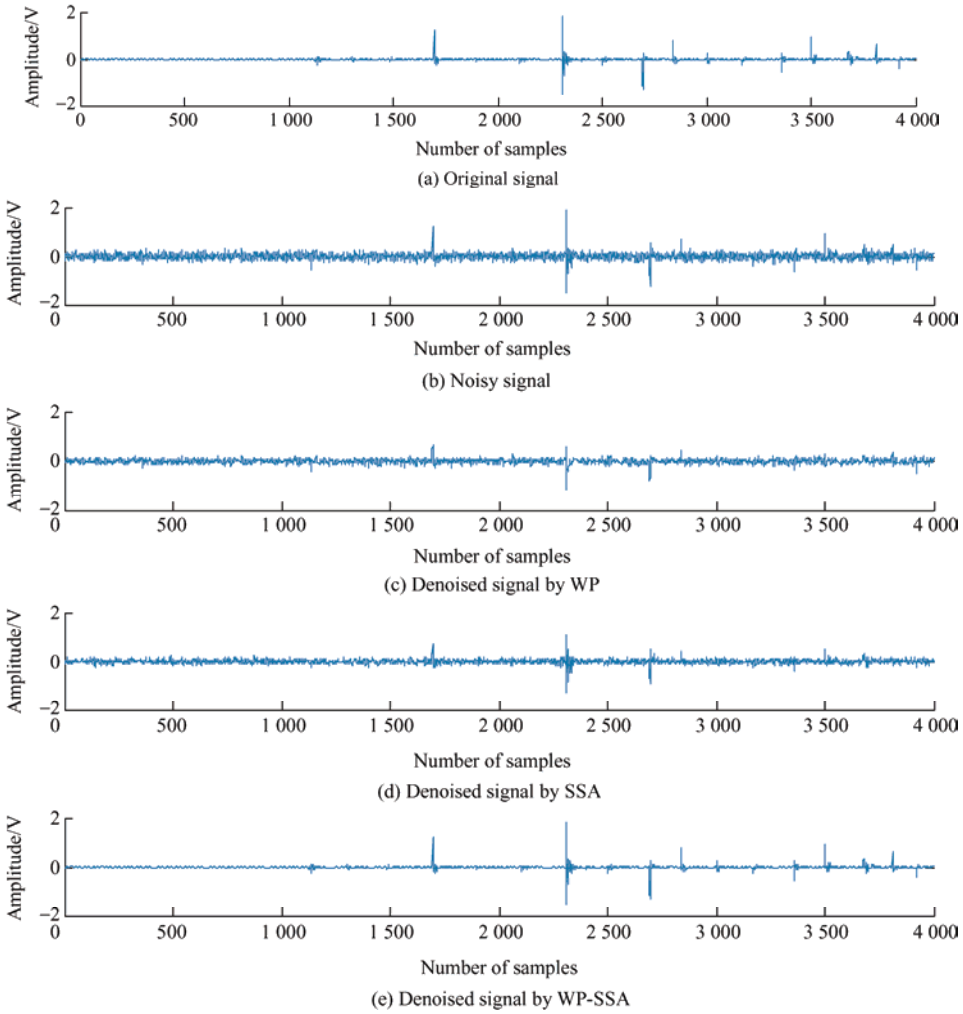

Fig. 3 Denoising effect comparison

As shown in Fig. 3, the denoising method proposed in this study has a better denoising effect than any single denoising method of WP and SSA. After denoising with WP-SSA, the obtained signal in Fig. 3a is nearly the same as the original signal shown in Fig. 3e. The vibration signal collected from the experimental platform is then preprocessed with the proposed WP-SSA for denoising. To reflect the denoising effect, the signal-to-noise ratio (SNR), correlation coefficient R, and root mean square error (RMSE) are calculated for the WP, the SSA, and the WP-SSA, respectively; the results are shown in Tab. 7.

Tab. 7 Denoising effect of vibration signal with different denoising methods

Denoising method	SNR	R	RMSE
WP	1.687	0.746	0.103
SSA	1.942	0.806	0.097
WP-SSA	2.942	0.916	0.089

The calculation formulas for the SNR, correlation coefficient, and RMSE are given by Eqs. (3)-(5) [23]

$$\mathrm{SNR}=10\times\lg\left(\frac{\sum_{i=1}^{N}y^2(i)/N}{\sum_{i=1}^{N}[f(i)-y(i)]^2}\right) \tag{3}$$

$$R=\frac{Cov(f_i,y_i)}{\sigma_{f_i}\sigma_{y_i}} \tag{4}$$

$$\mathrm{RMSE}=\sqrt{\frac{1}{N}\sum_{i=1}^{N}[f(i)-y(i)]^2} \tag{5}$$

where $f(i)$ is the noisy signal, and $y(i)$ is the signal after noise reduction. The larger SNR, the closer the R value is to 1; the smaller RMSE [24], the better the denoising effect of WP-SSA.

As shown in Tab. 7, the secondary denoising method of WP-SSA proposed in this study is superior to the simple WP or SSA, which verifies the effectiveness of the denoising method proposed herein.

3.2 EEMD-based signal feature extraction

After denoising with WP-SSA, the preprocessed signal is decomposed with EMD and EEMD to generate the intrinsic mode function (IMF) [25]. The decomposition effects of the EMD and EEMD are shown in Figs. 4 and 5, respectively.

As shown in Figs. 4 and 5, the EEMD not only improves the modal aliasing effect that occurs during signal decomposition, but also has a better decomposition effect than EMD.

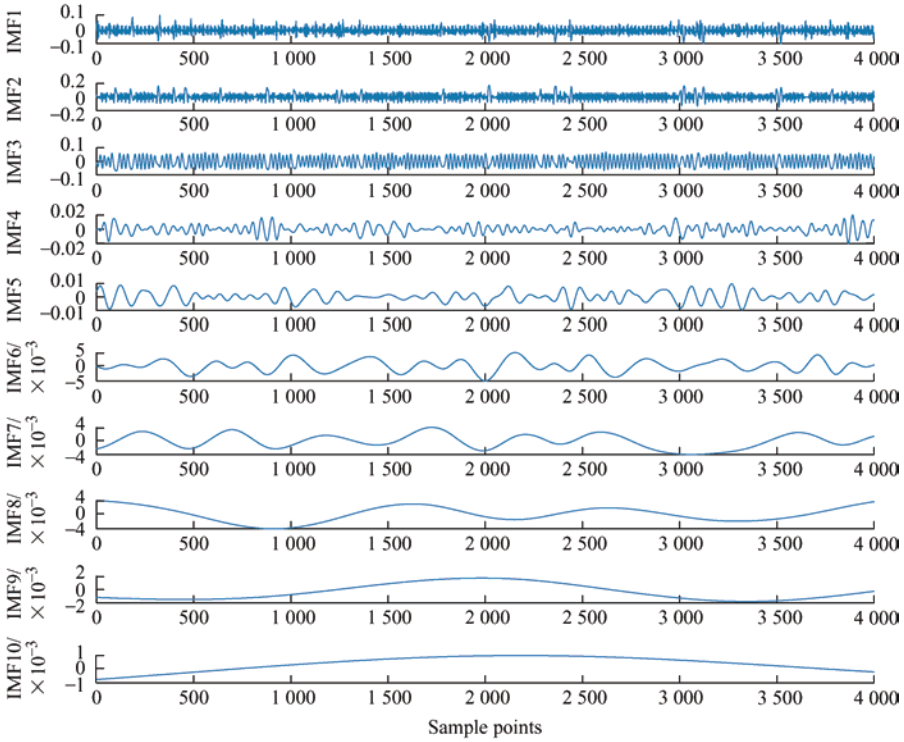

Fig. 4 EMD decomposition effect of signals after denoising

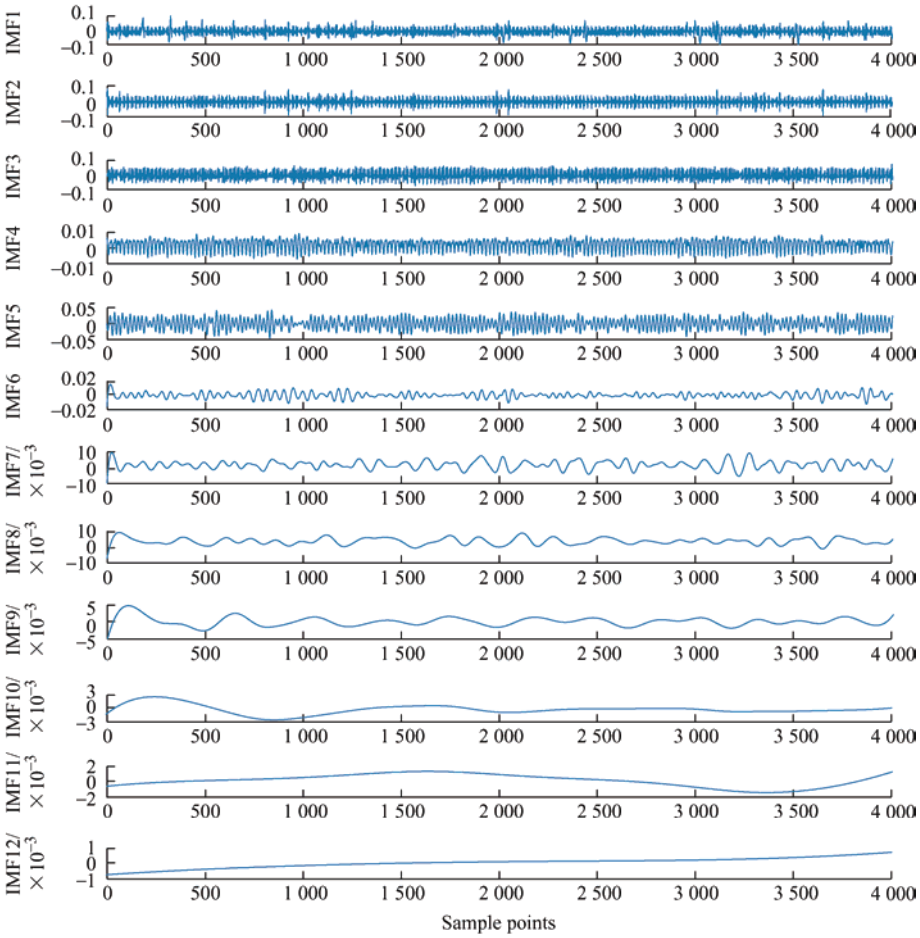

Fig. 5 EEMD decomposition effect of signals after denoising

Once the IMF is obtained from the measured signal, the Hilbert transform is applied to generate the corresponding Hilbert spectrum using the following equation [26]

$$H(\omega,t)=\mathrm{Re}\sum_{i=1}^{n}a_i(t)\exp\left(j\int\omega_i(t)\mathrm{d}t\right) \tag{6}$$

where $H(\omega,t)$ is the relationship between the signal amplitude, frequency, and time over the entire frequency range of the signal, ω is the frequency, t is time, a indicates the IMF; i=1, 2, ⋯, n, is the decomposition number of EEMD.

By integrating the Hilbert spectrum on the time axis, the Hilbert marginal spectrum can be finally obtained through Eq. (7) as follows [27]

$$h(\omega)=\int_0^T H(\omega,t)\mathrm{d}t \tag{7}$$

where T is the length of the signal sequence, $H(\omega,t)$ is the relationship between the signal amplitude, frequency, and time in the entire frequency range of the signal, and $h(\omega)$ is the relationship between the signal amplitude and frequency in the entire frequency range of the signal.

The generated Hilbert marginal spectra are shown in Fig. 6, which demonstrates that the marginal spectrum waveforms of the OLTC contact simulation device under normal and contact failure conditions are approximately the same between 0 Hz to 60 Hz.

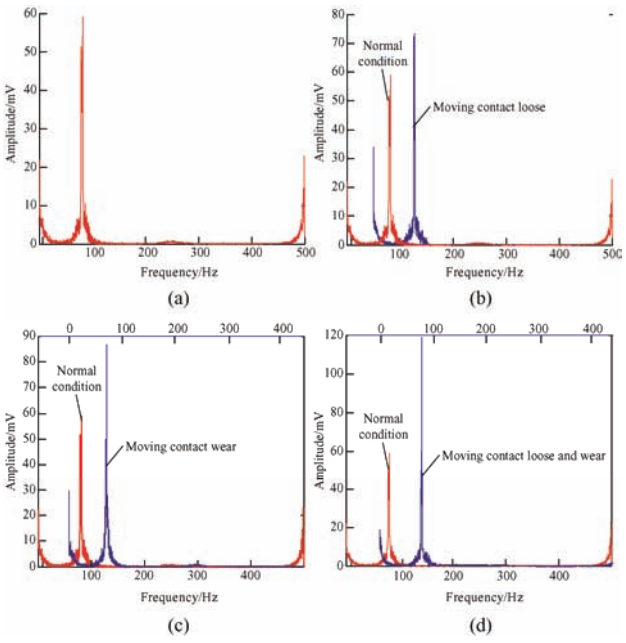

Fig. 6 Marginal spectrum of the normal signal and fault signal of the contact after denoising

However, the marginal spectral amplitude of the vibration signal in the abnormal state is significantly higher than that under the normal state between 60 Hz and 110 Hz, as shown in Figs. 6b, 6c, and 6d. Therefore, according to the Hilbert marginal spectrum, when the OLTC enters an abnormal state, the amplitude of the Hilbert marginal spectrum will exhibit a larger increase compared to the normal state.

3.3 Abnormal state detection using GWO-FCM

The FCM algorithm is a clustering algorithm based on an iterative optimization of the objective function [28]. By optimizing the objective function, the membership degree of each data point to all the clusters is obtained, and each data point is determined to achieve the classification purpose of this algorithm. The objective function of the FCM clustering algorithm $J(U, P)$ is defined as follows [29]

$$J(U,P)=\sum_{i=1}^{c}\sum_{j=1}^{n}(u_{ij})^{m}(d_{ij})^{2} \tag{8}$$

where c is the number of clusters, n is the number of samples, and m is the fuzzy index. Usually, the value is $m \in [1, 2.5]$. In this study, m=2, u_{ij} is the membership degree of sample j to category i, d_{ij} represents the Euclidean distance, that is, the distance between sample j and the cluster center i, which is defined as follows

$$(d_{ij})^{2}=\left\|x_i-p_j\right\|^{2} \tag{9}$$

where x_i indicates the i-th sample number, and p_j indicates the j-th cluster center.

During each iteration of optimizing the objective function, the corresponding membership values can be obtained through the membership function, from which a new membership matrix u_{ij} and various cluster centers c_i can be calculated.

Considering that the initial clustering centers of the FCM are generated randomly during the clustering process and cannot go beyond the limit of local convergence, which results in poor clustering performance, this study proposed the use of the GWO algorithm to optimize the FCM algorithm. The GWO is a swarm intelligence optimization algorithm proposed by Mirjalili et al. [30] in 2014, which is inspired by the hunting behavior of gray wolves. The GWO algorithm is used to describe the social hierarchy and hunting behavior of gray wolf populations. The social hierarchy is generally divided into four categories, denoted as α, β, δ, and ω [31]. Among these, α is the best wolf, β and δ are the second and third best wolves, respectively, while ω indicates the remaining wolves. The aim of the GWO algorithm is to determine the optimal solution within the specified range through the α, β, and δ wolves, and lead the ω wolf to update the position and finally complete the hunting behavior. The specific process is as follows [31].

When a gray wolf begins to search for its prey, the distance between the gray wolf and its prey can be expressed as follows

$$\boldsymbol{D}=\left|X_p(k)\left(\boldsymbol{C}-1\right)\right| \tag{10}$$

$$X_p(k+1)=X_p(k)-\boldsymbol{A}\boldsymbol{D} \tag{11}$$

$$\boldsymbol{A}=a\left(2r_1-1\right) \tag{12}$$

$$\boldsymbol{C}=2r_2 \tag{13}$$

where k is the number of iterations, $X_p(k)$ is the position vector of the prey, $X(k)$ is the position vector of the gray wolf, $\boldsymbol{D}$ is the distance vector between the gray wolf and the prey, and $\boldsymbol{A}$ and $\boldsymbol{C}$ are the coordination coefficients. Among these, the value of a is [0, 2], and linearly decreases from 2 to 0 in the iterative process; r_1 and r_2 are random vectors between [0, 1].

Gray wolves have the ability to identify the location of their prey and to encircle the prey during hunting. In each iteration of GWO, the three optimal solutions of α, β, and δ wolves are retained. The positions of the remaining ω wolves are then updated according to their positions, and the optimal solution is finally determined. The mathematical expression is as follows [31]

$$D_\alpha=\left|C_3X_\delta-X\right| \tag{14}$$

$$D_\beta=\left|C_2X_\beta-X\right| \tag{15}$$

$$D_\delta=\left|C_3X_\delta-X\right| \tag{16}$$

$$X_1=X_\alpha-A_1D_\alpha \tag{17}$$

$$X_2=X_\beta-A_2D_\beta \tag{18}$$

$$X_3=X_\delta-A_3D_\delta \tag{19}$$

$$X(k+1)=\frac{X_1+X_2+X_3}{3} \tag{20}$$

In the clustering process of FCM, the initial clustering center is randomly generated and cannot escape the limitation of local convergence, thus influencing its clustering performance. By using GWO to improve the FCM clustering algorithm, the aforementioned problems can be solved. As an efficient global search algorithm, GWO not only solves the local convergence problem but can also determine the optimal clustering center to minimize the objective function value of FCM, as well as obtain the best clustering result. The specific implementation process is as follows.

(1) Initializing the gray wolf population through the following equation

$$x_{i,j}=lower_j+(upper_j-lower_j)\times rand(0,1) \tag{21}$$

where i= (1, 2,⋯, n), j= (1, 2,⋯, d); $upper_j$ and $lower_j$ indicate the maximum and minimum values of the j element, respectively; n represents the population number, and d indicates the population dimension.

(2) Setting the fitness function by the objective function. In the FCM clustering process, the objective function value is negatively correlated with the clustering effect. When the objective function value J decreases, the clustering effect gradually improves. The fitness function is as follows

$$fitness=J^{-1} \tag{22}$$

Obviously, when the objective function J is smaller and the clustering effect is better, the fitness function of GWO is larger.

(3) Continuously iterating the parameters of α, β, and δ in the GWO algorithm to obtain the optimal fitness function value α, which is taken as the new clustering center of FCM to improve the clustering performance.

The vibration signal processed by EEMD and the Hilbert transform is used as the input of the K-means clustering [32], FCM clustering, and GWO-FCM clustering algorithm; the number of samples in the dataset is 4 000, the K value in the K-means clustering is set to 3, and the fuzzy index of the FCM clustering is chosen as 2. In Eq. (8), the original objective function is determined and the cluster center is randomly provided. Then, the objective function and cluster center are optimized through repeated iterations until the iteration termination condition is satisfied. Finally, the GWO-FCM cluster center matrix is obtained as follows

$$\boldsymbol{C}=\begin{bmatrix} 613.434\,2 & 44\,104.594\,7 & -0.043\,7 \\ 1\,999.499 & 44\,103.932\,5 & -0.001\,4 \\ 3\,385.565\,4 & 44\,103.930\,9 & -0.001\,2 \end{bmatrix}$$

The number of iterations for the objective function optimization is 159, and the final objective function output value is obj_fcn = 4.458 8×10^8. The clustering results obtained using K-means clustering, FCM, and GWO-FCM are provided in Figs. 7-9.

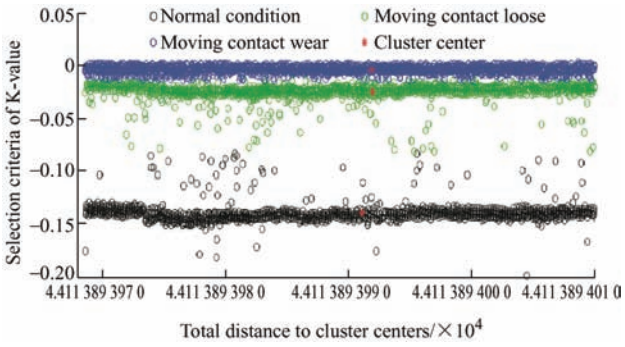

Fig. 7 K-means clustering result of experimental data

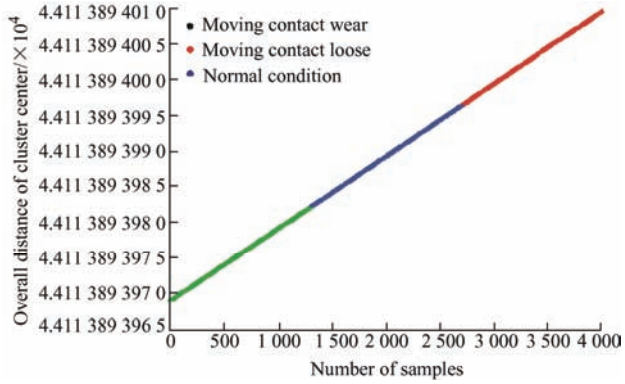

Fig. 8 FCM clustering result of experimental data

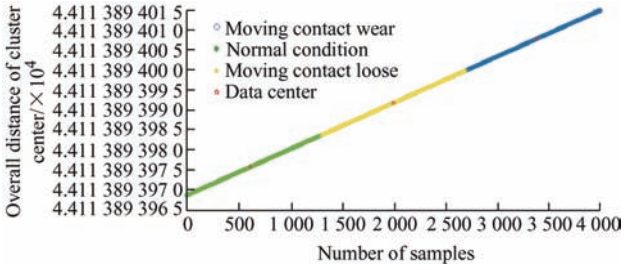

Fig. 9 GWO-FCM clustering result of experimental data

As shown in Fig. 7, the K-means clustering algorithm roughly divides the input vibration signal into three regions. The divisions are made according to the overall distance of the cluster center, from large to

small, the moving contact wear and contact loosening fault states, and the contact normal working state. In contrast, the FCM clustering and the GWO-FCM clustering divide the input vibration signal into three obvious areas, as shown in Fig. 8 and Fig. 9. It is clear that the FCM clustering and GWO-FCM clustering algorithms have better clustering results compared to the K-means clustering algorithm. Among these, GWO-FCM clustering has the best clustering performance compared to FCM clustering with clear cluster centers and clustering results.

To demonstrate the effectiveness of the GWO-FCM clustering algorithm more specifically, this study adopts the partition coefficient (PC) and partition entropy (PE) as the clustering performance evaluation index [33]. The system clustering effect, K-means clustering effect, and FCM clustering effect are evaluated, the results of which are shown in Tab. 8. Here, the closer the PC value is to 1 and the PE value is to 0, the higher the clustering efficiency. The PC and PE can be calculated using Eqs. (23) and (24), respectively.

$$\mathrm{PC}=\frac{1}{n}\sum_{i=1}^{c}\sum_{j=1}^{n}u_{ij}^{\ 2} \tag{23}$$

$$\mathrm{PE}=-\frac{1}{n}\left[\sum_{i=1}^{c}\sum_{j=1}^{n}u_{ij}\log_a(u_{ij})\right] \tag{24}$$

where $a\in[1,+\infty]$.

Tab. 8 Evaluation index of clustering algorithms

Clustering algorithm	PC	PE
Traditional clustering	0.798 9	0.140 2
K-means clustering	0.819 7	0.124 9
FCM clustering	0.854 9	0.106 4
GWO-FCM clustering	0.946 2	0.086 9

As shown in Tab. 8, the GWO-FCM clustering algorithm is better than the FCM and K-means clustering algorithms with respect to the PC and PE values. This confirms that the method proposed in this study provides an effective classification in the abnormal state detection of the OLTC experimental test signals.

4 Verification with onsite measured data

To verify the feasibility of the method proposed in this study, the OLTC switching vibration signals were collected from a transformer in a local substation. The sampling rate and the number of sampling points were consistent with the parameters set in the experiment test introduced in Section 3. The collected OLTC switching vibration signals were first preprocessed by the WP-SSA, and then the IHHT was implemented to extract the features of the denoised signal. The Hilbert marginal spectrum of the onsite collected normal operating OLTC switching signal after processing is provided in Fig. 10.

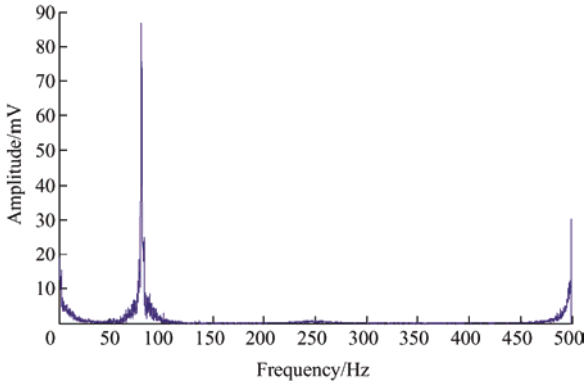

Fig. 10 Hilbert marginal spectrum of field collected data during OLTC switching

As shown in Fig. 10, the marginal spectral amplitude of the vibration signal is higher than that of the normal state and is lower than that of the fault state between 60-110 Hz. The OLTC is suspected to have certain faults; however, the fault types need a further diagnosis. Finally, the K-means, FCM, and GWO-FCM clustering algorithms are used to obtain a diagnosis of the vibration signal. The diagnosis results are shown in Figs. 11-13.

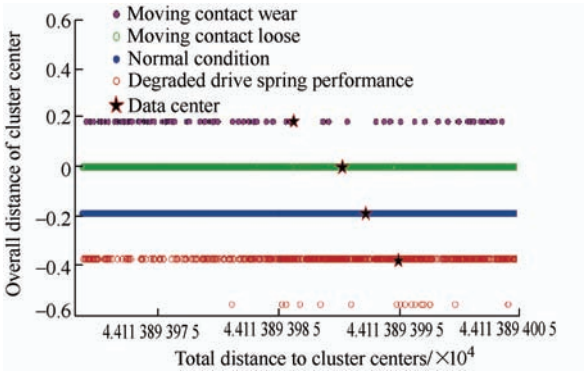

Fig. 11 K-means clustering results of field data

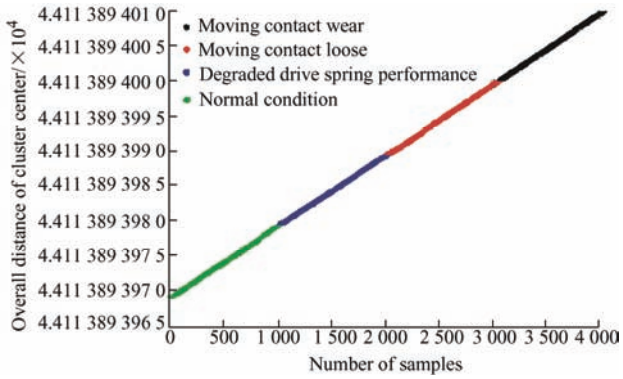

Fig. 12 FCM clustering results of field data

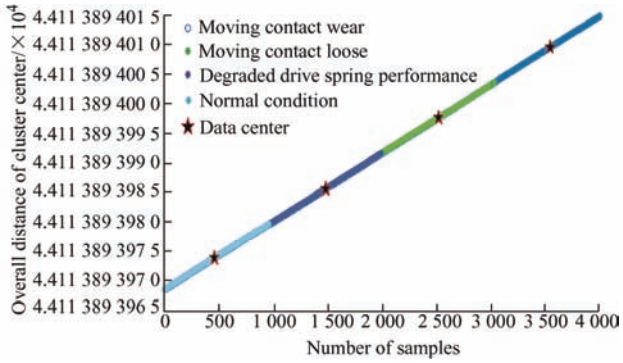

Fig. 13 GWO-FCM clustering results of field data

By comparing and analyzing the results in Figs. 11-13, the vibration signal of the transformer OLTC tested onsite consists of the following four states: wear of the moving contact, moving contact loosening, performance degradation of drive spring, and normal state. The proposed GWO-FCM clustering method has a better classification performance than FCM clustering and K-means clustering, which also verifies the feasibility of the proposed method for onsite application.

5 Conclusions

This article proposes an improved FCM method for abnormal state detection with both laboratory measured OLTC signals and onsite collected real OLTC switching signals. With the proposed method, the abnormal states of the OLTC can be detected through a series of processes including signal collection, preprocessing, feature extraction, and fault diagnosis. The following conclusions can be summarized based on the results presented in this study.

(1) The WP-SSA secondary denoising method proposed in this study solves the problem of WP neglecting small disturbances in the denoising process and improves the denoising effect of the vibration signals.

(2) By using the EEMD method, the modal aliasing effect that is easily generated when EMD decomposes vibration signals with Gaussian white noise is improved, thereby improving the accuracy of the vibration signal feature extraction.

(3) The GWO-FCM clustering algorithm has a better clustering performance than the K-means clustering and FCM clustering algorithms, which improves the abnormal state detection for the OLTC and also provides a reliable basis for online monitoring and fault diagnosis of an actual transformer OLTC.

References

[1] D J Rogers, T C Green. An active-shunt diverter for on-load tap changers. *IEEE Transactions on Power Delivery*, 2013, 28(3): 649-657.

[2] J J Erbrink, E Gulski, J J Smit, et al. Diagnosis of on load tap changer contact degradation by dynamic resistance measurements. *IEEE Transactions on Power Delivery*, 2010, 25(2): 2121-2131.

[3] Q M Li, T Zhao, L Zhang, et al. Mechanical fault diagnostics of on-load tap changer within power transformers based on hidden Markov model. *IEEE Transactions on Power Delivery*, 2012, 27(6): 596-601.

[4] G S Liang, L T Wang, F Gao, et al. A new maximum step voltage calculation method of on-load tap-changer for symmetrical two-core phase shifting transformer. *IEEE Transactions on Power Delivery*, 2018, 33(4): 2718-2725.

[5] L J Chen, T P Tsao, Y H Lin. New diagnosis approach to epoxy resin transformer partial discharge using acoustic technology. *IEEE Transactions on Power Delivery*, 2005, 20(5): 501-508.

[6] J Seo, H Ma, T K Saha. A joint vibration and arcing measurement system for online condition monitoring of on load tap changer of the power transformer. *IEEE Transactions on Power Delivery*, 2017, 32(2): 1031-1038.

[7] P J Kang, D Birtwhistle. Condition assessment of power transformer on-load tap changers using wavelet analysis. *IEEE Transactions on Power Delivery*, 2001, 16(3): 394-400.

[8] M Y Zhao, G Xu. Feature extraction of power transformer vibration signals based on empirical wavelet transform and multiscale entropy. *IET Science Measurement & Technology*, 2018, 12(5): 63-71.

[9] E E Abraham, H Marzooghi, J Yu, et al. A novel adaptive supervisory controller for optimized voltage controlled demand response. *IEEE Transactions on Smart Grid*,

2019, 10(4): 4201-4210.

[10] Z H Li, Q H Li, Z T Wu, et al. A fault diagnosis method for on load tap changer of aerospace power grid based on the current detection. *IEEE Access*, 2018, 6: 24148-24156.

[11] R C Duan, F H Wang. Fault diagnosis of on-load tap-changer in converter transformer based on time-frequency vibration analysis. *IEEE Transactions on Industrial Electronics*, 2016, 63(3): 3815-3823.

[12] D Min, J Heo, K Hur, et al. Setting parameters of the analytic wavelet transforms for estimating electric power system damping parameters. *IEEE Transactions on Power Delivery*, 2012, 27(7): 2409-2411.

[13] H Chen, J Shen, W Chen, et al. The bivariate empirical mode decomposition and its contribution to grinding chatter detection. *Applied Sciences*, 2017, 7(6)：145-153.

[14] T S Xu, H D Chiang, G Y Liu, et al. Hierarchical K-means method for clustering large-scale advanced metering infrastructure data. *IEEE Transactions on Power Delivery*, 2017, 32(6): 609-616.

[15] L Si, Z Wang, C Tan, et al. Vibration-based signal analysis for shearer cutting status recognition based on local mean decomposition and fuzzy C-means clustering. *Applied Sciences*, 2017, 7(3): 164-175.

[16] W Zhao, X Y Xia, M D Li, et al. Online monitoring method based on locus-analysis for high-voltage cable faults. *Chinese Journal of Electrical Engineering*, 2019, 5(3): 42-48.

[17] D J Rogers, T C Green. An active-shunt diverter for on-load tap changers. *IEEE Transactions on Power Delivery*, 2013, 28(4): 649-657.

[18] T G Yi, Y Z Xie, H Y Zhang, et al. Insulation fault diagnosis of disconnecting switches based on wavelet packet transform and PCA-IPSO-SVM of electric fields. *IEEE Acces*s, 2020, 8: 176676-176690.

[19] X P Wang, B W Ling. Length reduction of singular spectrum analysis with guarantee exact perfect reconstruction via block sliding approach. *IEEE Access*, 2020, 8: 170311-170321.

[20] Z C Li, C Di, X H Bao. Analysis of vibration and noise of induction motor equipped with concentric single-double-layer star-delta winding. *Chinese Journal of Electrical Engineering*, 2019, 5(1): 36-46.

[21] X B Xu, M Zhang, M Z Luo, et al. Echo signal extraction based on improved singular spectrum analysis and compressed sensing in wavelet domain. *IEEE Access*, 2019, 7: 67402-67412.

[22] X Geng, L Ji, Y Zhao, et al. A small target detection method for the hyperspectral image based on higher order singular value decomposition (HOSVD). *IEEE Geoscience & Remote Sensing Letters*, 2013, 10(5): 1305-1308.

[23] S Qiu, J Feng, R Xu, et al. A stimulus artifact removal technique for SEMG signal processing during functional electrical stimulation. *IEEE Transactions on Biomedical Engineering*, 2015, 62(3): 1959-1968.

[24] M R Ram, K V Madhav, E H Krishna, et al. ICA-based improved DTCWT technique for MA reduction in PPG signals with restored respiratory information. *IEEE Transactions on Instrumentation & Measurement*, 2013, 62(3): 2639-2651.

[25] Z H Wu, N E Huang. Ensemble empirical mode decomposition: A noise-assisted data analysis method. *Advances in Adaptive Data Analysis*, 2008, 1(2): 31-41.

[26] N E Huang, S R Long, S Zheng. A new view of nonlinear water waves: The Hilbert spectrum. *Annual Review of Fluid Mechanics*, 1999, 31(3): 457-471.

[27] C Li, G Yu, B Fu, et al. Fault separation and detection for compound bearing-gear fault condition based on decomposition of marginal Hilbert spectrum. *IEEE Access*, 2019, 77: 110518-110530.

[28] F Zhao, Y L Chen, H Q Liu, et al. Alternate PSO-based adaptive interval type-2 intuitionistic fuzzy C-means clustering algorithm for color image segmentation. *IEEE Access*, 2019, 7: 64028-64039.

[29] J B Xiong, X Liu, X T Zhu, et al. Semi-supervised fuzzy C-means clustering optimized by simulated annealing and genetic algorithm for fault diagnosis of bearings. *IEEE Access*, 2020, 8: 181976-181987.

[30] S Mirjalili, S M Mirjalili, A Lewis. Grey wolf optimizer. *Advances in Engineering Software*, 2014, 69(3): 46-61.

[31] S Arora, H Singh, M Sharma, et al. A new hybrid algorithm based on grey wolf optimization and crow search algorithm for unconstrained function optimization and feature selection. *IEEE Access*, 2019, 7: 26343-26361.

[32] L Xie, H W Li, Y Yuan, et al. Line loss calculation method based on K-means clustering and improved multi classification relevance vector machine. *Journal of Electrical Engineering*, 2021, 16(1): 62-69.

[33] Y F Li, X Q Zuo, F Yang. Research on urban resident activity patterns and hotspot area based on GPS floating car data. *IEEE Access*, 2020, 8: 2694-2707.

Hongwei Li born in Gansu, China, 1981. He received his bachelor's and master's degree in Lanzhou Jiaotong University in 2003 and 2009 respectively, both majoring in Traffic Information Engineering Control. From 2003 to 2012, he was a Research Engineer with the School of Automation and Electrical Engineering in Lanzhou Jiaotong University, where he was engaged in the research of control of wind generation systems. Since August 2012, he has been studying for his Ph.D. His current research interests are in the areas of coordination control of subsystems of wind turbine.

Lilong Dou was born in Gansu, China, in 1994. He received the B.Sc. degree from Lanzhou Jiaotong University, Lanzhou, China, in 2019. He is currently working toward the M.Sc. degree at Lanzhou Jiaotong University, Lanzhou, China. His research interests include condition monitoring and fault diagnosis of transformer on load tap changer.

Shuaibing Li (S'14-M'19, IEEE) was born in Gansu, China, in 1989. He received the B.Sc. degree in Automation in 2011, and M.Sc. degree in Control Theory and Control Engineering in 2014 from Lanzhou Jiaotong University, and the Ph.D. degree in Electrical Engineering in 2018 from Southwest Jiaotong University. Now, he is a Lecture with the School of New Energy and Power Engineering, Lanzhou Jiaotong University. He is also the PI of the Institute of New Energy Power Systems (INEPS), Lanzhou Jiaotong University. His research interests include information processing, condition monitoring, assessment and fault diagnosis of high-voltage power equipment, and dynamic state estimation of electrical power systems.

Yongqiang Kang (M'17, IEEE) was born in Gansu, China, in 1988. He received the B.Sc. and M.Sc. degree in Control Theory and Control Engineering in Electrical Engineering from Lanzhou Jiaotong University, Lanzhou, China, in 2008 and 2012, respectively, and the Ph.D. degree in Electrical Engineering in 2019 from Southwest Jiaotong University. His research interest includes gas discharge.

Xingzu Yang was born in Hebei，China，in 1996. He graduated from Beijing University of Civil Engineering and Architecture in June 2019 with a B.Sc. degree in Building Electrical and Intelligent major. Currently he is a master degree candidate in the Lanzhou Jiaotong University，under the guidance of Lecturer Li Shuaibing．And presently his main research field is derivation mechanism of contact resistance of oil-immersed on-load tap-changer.

Haiying Dong (M'20, IEEE) was born in Shanxi, China, in 1966. He received the B.S. M.S. and Ph.D. degrees from the Beijing University of Aeronautics and Astronautics, Lanzhou Railway Institute, and Xi'an Jiaotong University, respectively. He is currently a Professor and Ph.D. supervisor with the School of New Energy and Power Engineering, Lanzhou Jiaotong University. Currently, he is the Dean of the School of New Energy and Power Engineering. He has published more than 80 journal papers and been authorized 10 patents. His research interests include condition diagnosis of high-voltage power equipment, optimal operation and intelligent control of power systems, and optimal control of new energy generation.